Thermally Induced Breakup of Levitated Droplet

A. Saha[1], S. Basu[2*], R. Kumar[1]
[1]University of Central Florida, Orlando, USA
[2]Indian Institute of Science, Bangalore, USA
abhishek.saha@ucf.edu, sbasu@mecheng.iisc.ernet.in and ranganathan.kumar@ucf.edu

Abstract

We report two kinds of instabilities in the form of secondary atomization and catastrophic breakup in levitated fuel droplets. The short wavelength (Kelvin-Helmholtz) instability for diesel and bio-diesel triggers secondary atomization near the droplet equator. Temperature dependent fuel properties and external heating rate are responsible for the inception and relative strength of these instabilities. If breakup occurs, it is always preceded by secondary atomization when droplet Weber number exceeds a critical value. The second type of instability results from change in surface tension and viscosity with increase in droplet temperature which causes wide fluctuations in droplet aspect ratio. If the viscous damping of aspect ratio oscillation is not strong enough, the droplet goes through unbounded stretching. A stability criterion has been established based on the inhomogeneity of Bernoulli (acoustic) pressure and surface tension of the droplet in terms of a local Weber number and Ohnesorge number. This instability is thermally induced in a droplet which does not experience instabilities without external heating.

Introduction

Interaction of fluid flow with an external acoustic field has been an important field of study for its wide range of applications in both micro and macro scales such as flame stability in combustion [1], atomization and generation of liquid droplets [2], and ultrasonic levitation [3-6]. Results have been reported on the generation of droplets from the long range capillary waves using ultrasound [2, 7-9]. The physics of ultrasonic atomization of fuels in the presence of a surface tension gradient and temperature dependent properties is not treated in these studies, particularly for vaporizing droplets subject to significant external heating.

In this work, we study the thermal effects that lead to possible instability and break up observed in acoustically levitated fuel droplets. Our observations clearly illustrate that under certain conditions, heated droplets are susceptible to two distinct modes of instability: a) short wavelength Kelvin-Helmholtz instability that pinches into satellite droplets at the equator but triggers no significant transient shape change, and b) long wavelength capillary wave instability that leads to significant variation in droplet aspect ratio and eventually to catastrophic breakup of the droplet. We report this unexpected finding that the temperature-dependent fuel properties and external heating rate may be exploited to provide insight into the relative strength of these two instabilities. Depending on the surface tension and viscosity gradients with temperature, either or both or no instabilities can occur in a droplet. Furthermore, the secondary atomization caused by short range pinching at the droplet equator always precedes the capillary waves that trigger bulk breakup, if both instabilities were to occur. We provide the criteria for the occurrence of such instabilities. Without external heating, no instabilities are observed throughout the entire lifetime of the droplet. In this paper, we focus on the first type of instability that can be observed at the droplet equator. The second type of instability of long wavelength will be discussed and explained in a subsequent article.

	$T_S(^oC)^{\#}$	σ (mN/m)$^{\$}$	$d\sigma/dT$ (mN/m/K)$^{\#\#}$	μ(cP)$^{\$}$	P_{sat}/P_{atm} $^{\$}$	ρ_l(kg/m^3) $^{\$\$}$	h_{fg}(kJ/kg) $^{\$\$}$
Kerosene	25 – 80	29.1 - 22.0	-0.117	1.82 - 0.85	$4.33x10^{-3}$ - $4.38x10^{-2}$	790	322.2
Ethanol	25 – 60	22.5 - 19.4	-0.088	1.36 - 1.02	$2.28x10^{-1}$ - $6.15x10^{-1}$	789	904
Diesel	25 – 80	31.6 - 23.9	-0.140	2.81 - 1.60	$1.49x10^{-3}$- $1.13x10^{-2}$	760	588.7
Bio-diesel	25 – 90	31.7 - 23.0	-0.123	4.60 - 1.70	$4.49x10^{-9}$-$1.01x10^{-5}$	787	254

$^{\#}$: initial and final temperature, $^{\$}$: determined at initial and final temperature, $^{\#\#}$: averaged over the temperature range observed during the experiment, $^{\$\$}$: at initial temperature

Table I: Temperature dependent property values for the fuels. T_s: surface temperature, σ: surface tension, μ: dynamic viscosity, P_{sat}: vapor pressure, ρ_l: liquid density, h_{fg}: latent heat

Experimental Setup

The current work uses a similar experimental setup described previously [4-6]. A 100 kHz acoustic levitator with amplitude of 156 dB (SPL) was used to suspend the droplets. The droplets were generated at the levitator pressure node

using a micro syringe. A CO_2 laser with a beam diameter of 4 mm, lasing at 10.6 μm has been used to heat the droplet. The heating event has been recorded simultaneously by a high speed camera whose images were processed to obtain instantaneous diameter, aspect ratio and shape changes, and an infra-red (IR) camera to obtain the surface temperature of the droplet. Both cameras use microscopic lenses to increase the spatial resolution. The high speed camera was operated at 3000-10000 fps, while the IR camera was operated at 100 fps.

Results and Discussion

Pure liquid droplets of four different fuels namely ethanol, diesel, kerosene, bio-diesel were levitated. The droplets had initial diameter of 500 +/- 15 μm and were irradiated with 1.25 MW/m^2 heat flux. The radiative heating causes a sharp regression in droplet diameter (Figure 1) for the initial 0.2s. The diameter reduction rate is fastest for ethanol, while kerosene, diesel and bio-diesel vaporize slowly. The ethanol vapor pressure is higher (Table I) compared to the other three fuels, leading to a faster vaporization rate. The surface temperature of the droplet (Figure 1) is analogous to the wet-bulb temperature of a vaporizing droplet in a hot gas medium, and is low at the onset of heating; however as the vapor pressure of the liquid increases with temperature, the evaporation rate increases. Faster vaporization progressively requires higher amount of latent heat thereby reducing the available sensible heat responsible for temperature rise. Maximum temperature is reached at equilibrium, which depends on the heating rate, vapor pressure, latent heat and specific heat of the fuel. It is lowest (60^{o}C) for ethanol and highest (95^{o}C) for bio-diesel. Both kerosene and diesel exhibit maximum temperature of 80^{o}C.

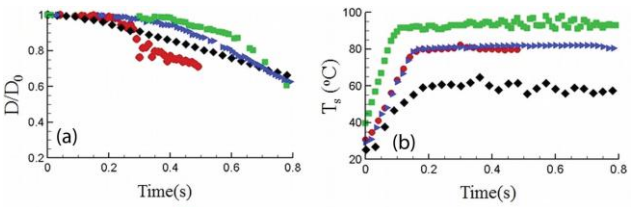

Figure 1: a) non-dimensional diameter (D/D_0), b) Average surface temperature (T_s)

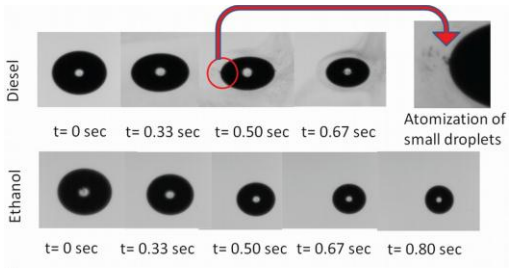

Figure 2: High speed images of atomization [diesel: atomization, Ethanol: no atomization

After 0.3-0.4s of heating, we observe different types of instabilities arising in kerosene, diesel and bio-diesel droplets. These fuels start atomizing from the equator in the form of small droplets of sizes ~1-10 μm (Figure 2). This is a short wavelength instability that pinches tiny droplets at the equator. At the onset of this secondary atomization, the diameter reduction becomes a cumulative outcome of two events, i.e., evaporation and small scale atomization for all three fuels. Ethanol droplet, on the other hand, does not exhibit any atomization, hence the slower diameter reduction rate. We will discuss other events related to kerosene in the next article.

KH instability

The classical Kelvin-Helmholtz (KH) type instability sets in when the relative motion between the levitated droplet and the surrounding air exceeds a critical value. This depends on the surface tension and density of the fluids [10]:

$$u_{crit}^2 = [2(\rho_l + \rho_0)/\rho_l\rho_0]\sqrt{\sigma.(\rho_l - \rho_0).g} \quad (1)$$

where ρ_l and ρ_0 are densities of liquid and air respectively, σ is surface tension, g is acceleration of gravity. The relative velocity can be approximated by the acoustic streaming velocity, u_{str}. For KH-instability, $u_{str} > u_{crit}$ condition has to be satisfied. In general the KH instability is the instability between gravitational force and shearing force due to relative motion between two fluid layers. In a levitated droplet, this can be extended to the instability between shear force due to acoustic streaming velocity at the droplet surface and net downward or upward force acting on the droplet, which can be scaled as 'g' (gravitational acceleration). Although the net force may be different on the top and bottom sectors of the droplet, the critical condition always occurs near the equator, as it has the smallest radius of curvature (explained later) and at this point the shear force due to streaming velocity (which is parallel to droplet surface) and the net gravitational force will act against each other leading to maximum instability. The acoustic streaming velocity is expressed as,

$$u_{str} = P_0\gamma_0 Ma/\rho_0 c_0 \quad (2)$$

where P_0 = atmospheric pressure; γ_0 = ratio of specific heats; ρ_0 =density of air stream around the droplet; c_0 =sonic velocity; Ma =acoustic Mach number. Mach number is directly related to the SPL (Sound Pressure Level) of the levitator (constant for the current experiment) by $SPL[dB] = 197 + 20\log(Ma)$. Note that the heated, vaporizing droplet will always be covered with a concentrated fuel vapor blanket. Moreover, the acoustic streaming around the droplet suppresses the natural diffusion process of this concentrated vapor blanket. It is necessary to include the effect of this

vapor blanket around the droplet while calculating the streaming velocity. From classical vaporization theory [11], one can calculate mass fraction ($Y_{l,s}$) of fuel vapor at the droplet surface

The effective density of the vapor film around the droplet is

$$\rho_{0,eff}(T_s) = \left[\frac{Y_{f,s}(T_s)}{\rho_{l,vap}(T_s)} + \frac{1-Y_{f,s}(T_s)}{\rho_{air}(T_s)} \right]^{-1}. \quad (3)$$

The streaming velocity can be redefined as

$$u_{str-eff} = \frac{P_0 \gamma_0 Ma}{\rho_{0,eff}(T_s) c_0} \quad (4)$$

which is a strong function of the vaporization characteristics of the different liquid fuels. In general, the criterion for droplet atomization events is defined in terms of Weber number, which is the ratio of pressure force and capillary force. In acoustically levitated droplet, the Weber number, $We = 8P_B / P_\sigma$, is defined as the ratio of Bernoulli's stress (pressure) and stress due to surface tension [9], which reduces to $We = 2P_0\gamma_0 Ma^2 R/\sigma$; Using an effective Mach Number,

$$Ma_{eff} = u_{str\text{-}eff}/c_0 \quad (5)$$

$$We_{eff} = \frac{2P_0\gamma_0 Ma_{eff}{}^2 R}{\sigma} = \frac{2P_0\gamma_0 (u_{str-eff}/c_0)^2 R}{\sigma} \quad (6)$$

We_{eff} is transient for a vaporizing droplet due to temperature dependent properties and fuel type. Without external heating, the effective Weber number exhibits dependence only on the droplet diameter and slow transient variations.

For KH instability, the critical Weber number for atomization is

$$We_{crit} = 2P_0\gamma_0 (u_{crit}/c_0)^2 R/\sigma \quad (7)$$

Since the small scale atomization only occurs at the droplet equator, it is more appropriate to use R_c (radius of curvature at the droplet equator) as the length scale to redefine We_{eff} and We_{crit}. The aspect ratio of the droplet changes dynamically as heating and vaporization progress with time (Figure 1). The shape of the droplet approximates to an ellipse, and its local radius of curvature at any point on the equator perimeter is $r_c = \frac{(b^2\cos^2 t + a^2 \sin^2 t)^{3/2}}{a.b}$; a and b are the major and minor axes; c(=a/b) is the aspect ratio, and 't' is calculated by $\varphi(t) = \tan^{-1}(\frac{a}{b}\tan t)$. φ is the polar angle with the ellipse center as origin. For φ =0 or π/2 at the equator, $R_c = b^2/a = b/c$. The criterion for atomization can be recast as $We_{eff} > We_{crit}$ where $We_{crit} = 2P_0\gamma_0 (u_{crit}/c_0)^2 R_c/\sigma$ and $We_{eff} = 2P_0\gamma_0 (u_{str-eff}/c_0)^2 R_c/\sigma$. The liquid surface tension is a function of temperature and the droplet size exhibits a transient regression with heating. This implies that We_{crit} and We_{eff} vary as $\sigma^{-1/2}$ and σ^{-1} during the droplet heating cycle, We_{eff} and We_{crit} will progressively decay as the droplet surface temperature increases and the difference $(We_{crit} - We_{eff})$ can decrease until the atomization criteria is satisfied. Therefore, for liquid droplets, with similar surface tension gradients, the probability of KH instability increases for higher surface temperature.

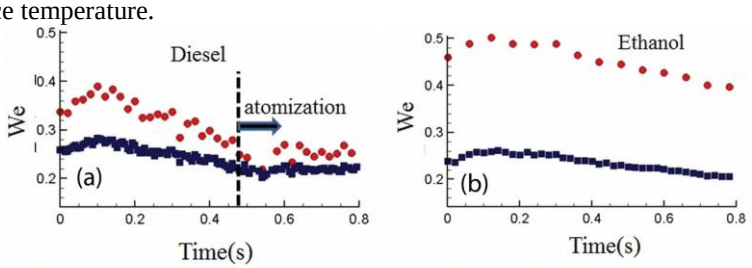

Figure 3: Critical Weber number (We_{crit}) and Effective Weber number (We_{eff})

Initially, We_{crit} is larger compared to We_{eff} for all fuels (Figure 3). For diesel and bio-diesel, high speed images corroborate the time at which We_{eff} converges to We_{crit} and atomization is triggered. Kerosene reaches this condition fastest (around 0.3 sec). In the absence of external heating, We_{crit} and We_{eff} would have exhibited a very slow change due to natural evaporation of the droplet. Thus, no atomization would be observed if there is no external heating. With heating, the vaporization pattern for each fuel droplet is different. The change in the temperature and diameter of a vaporizing droplet depends on the vapor pressure, latent heat and specific heat. The surface temperature and vapor pressure also dictate the change in vapor density around the droplet as explained earlier. Ethanol shows a low surface temperature, thereby reducing the possibility of KH instability.

In general, all droplets deform into an ellipsoidal shape and the oblateness or the aspect ratio is higher for the atomizing droplets (Figure 2). The theory of levitation [3, 9] suggests that the aspect ratio is dependent on levitator SPL, surface tension, density and droplet diameter. As mentioned earlier, the atomization occurs at the equator as it has minimum radius of curvature. For a given volume of droplet, the aspect ratio determines the radius of curvature at the equator. Parameters such as SPL and surface tension affect the aspect ratio and, in turn, affect the atomization. Increase in SPL and reduction in surface tension result in the augmentation of aspect ratio. However, both definitions of Weber numbers ($We_{crit} = 2P_0\gamma_0(u_{crit}/c_0)^2 R_c/\sigma$ and $We_{eff} = 2P_0\gamma_0(u_{str-eff}/c_0)^2 R_c/\sigma$) use the radius of curvature as the length scale. So the change in SPL which alters the radius of curvature would have the same effect on both the Weber numbers and hence would not change the instability criterion. On the other hand, the surface tension has separate and distinct effects on We_{crit} and We_{eff}. Change in surface tension would not only affect the aspect ratio but would also influence the Weber numbers directly. The change in aspect ratio (or radius of curvature) would create similar changes on both the Weber numbers as mentioned earlier. However, We_{crit} and We_{eff} show $\sigma^{-1/2}$ and σ^{-1} dependence. Surface tension decreases with temperature, leading to a sharper rise in We_{crit} than We_{eff} . It is difficult to conduct experiments with liquid droplet under external heating to demonstrate the effects of surface tension on KH instability, as the droplet will vaporize and create a vapor blanket around it, changing the streaming velocity and thereby altering We_{eff}. However, for liquids like kerosene (Figure 1), vaporization is not significant for the initial 200 msec, so the effect of the vapor blanket on streaming velocity would not be significant. Similarly, diesel also does not vaporize in the same duration, resulting in a sharp increase in temperature (up to 80°C), which reduces its surface tension. In the first 100 msec (Figure 3a), We_{crit} and We_{eff} increase by ~20% and ~10% respectively.

Catastrophic Breakup of Droplet:

In addition to KH induced atomization, kerosene experiences bulk deformation leading to bag type and capillary wave induced breakup. With progressive heating, the kerosene droplet initially gets stretched in the horizontal direction and subsequently morphs into a thin disk with a significant variation in aspect ratio and eventually undergoes breakup (Figure 4). It is to be noted that other fuels like biodiesel and diesel show shape changes but do not regress into a disk shaped morphology. This clearly suggests that general criterion maybe established to ascertain the stability of droplet based on the external acoustic pressure field, internal recirculation due to acoustic streaming and the variation of temperature dependent properties like viscosity and surface tension.

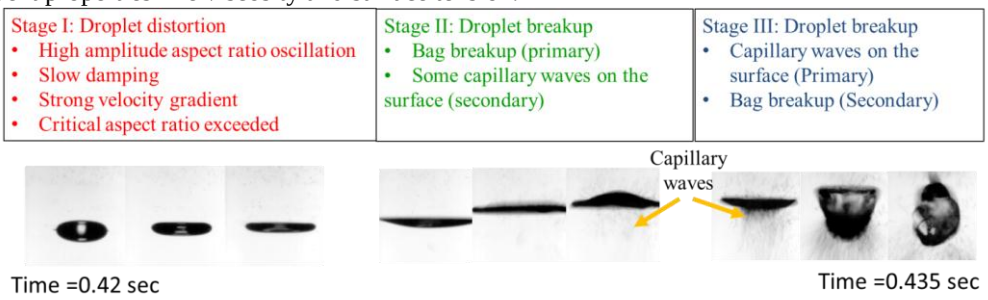

Figure 4: catastrophic breakup of kerosene droplet

As shown in Figure 4, the breakup process of a kerosene droplet occurs over 15 ms, and can be further subdivided into three stages. In Stage I, the levitated droplet deforms to a disk or pancake-shaped structure while displaying high amplitude oscillations in aspect ratio along with low damping and a high velocity gradient in the liquid phase. Subsequently in stage II, the droplet resembles a disc and blows up like a bag near the center. Stage III is marked by violent breakup of the bag along with capillary waves induced on the flattened surface of the deformed droplet. No atomization is observed in stage I, but it is marked by substantial distortion of the droplet which serves as a precursor to the eventual catastrophic breakup in stages II and III. Although this catastrophic break up begins to occur around 0.42 sec, this instability is triggered earlier when the temperature of the droplet increases due to radiative heating. All liquid droplets are subject to deformations under acoustic loading. However, only kerosene-like liquids reach the critical deformation limit necessary for breakup.

Stage I (Droplet Distortion Stage)

A levitated droplet takes the shape of an ellipsoid (c>1) due to the non-uniformity of the acoustic/Bernoulli pressure around the droplet [12]. The pressure force around the droplet deforms it and the surface tension force tends to restore the spherical shape. The amount of oblateness or the tendency to deviate from the spherical shape (c=1), depends on the fluid properties such as, density and surface tension. Hence, the mean aspect ratio can be written as $\bar{c} = f(\rho, \sigma)$. For stability the balance in external acoustic pressure force and maximum surface tension force (at the equator) can be expressed as,

$$P_{pole} - P_{eq} = \sigma / R_c \quad (8)$$

where P_{pole}-P_{eq} is the difference between the Bernoulli pressure at the pole (P_{pole}) and at the equator. Bernoulli pressure outside the droplet (P_{eq}) and R_c is the radius of curvature at the equator. P_{pole}-P_{eq} represents the appropriate scale for the external acoustic force that accounts for the local inhomogeneity of the pressure distribution due to shape change. Small perturbations in the external pressure field around the droplet also oscillates which triggers an oscillation in the aspect ratio. In our previous work [5, 12], we showed that the velocity field in a levitated spherical droplet is tangential in nature, i.e., $v_r = 0$, and that $v_\theta = (K.r)$, where K is a constant which depends on the droplet and levitator properties. With the departure from the spherical shape (aspect ratio, c>1), polar radius decreases, increasing the equatorial radius, which subsequently augments the fluid flow towards the equator resulting in the droplet getting stretched away from the center. So in a nutshell, Bernoulli pressure continues to deform any levitated droplet. However, in most cases, surface tension inhibits the Bernoulli pressure to continuously deform the droplet.

The radius if curvature at the equator is expressed $R_c = \frac{b}{c} = \frac{3V}{4\pi a^2 c}$ where V is volume of the droplet ($V = \frac{4}{3}\pi a^2 b$), a and b are polar and equatorial radii. So with increase in aspect ratio, R_c will decrease, which, in turn, will increase the surface tension pressure. Thus, the droplet shape continues to oscillate about a mean value. Fluid properties also play an important role in controlling the intensity of this oscillation. The fluid viscosity acts as a damping force on the velocity field. Higher viscosity reduces the flow towards the equator. Strong damping due to viscosity can, in essence, dissipate the high energy shape fluctuations (especially high amplitude modes of vibration) before it assumes catastrophic proportions.

For a small change in aspect ratio, δc, the change in critical radius can be written as $\delta R_c = -\frac{5}{3}\frac{R_c}{c}\delta c$. The Bernoulli pressure or the acoustic pressure which also changes with change in aspect ratio, can be expressed as $P(r,z) = P_{\max}\sin(k_z z).J_0(k_r r)$ where, $P_{\max} = P_0\gamma_0 Ma$ is constant in the current the experiment; P_0 is the atmospheric pressure, γ_0 is the specific heat ratio; Ma is the acoustic Mach number and r and z are radial and axial coordinate measured from the pressure node and J_0 is Bessel function of zeroth order. The droplet under gravity will be shifted downwards from the pressure node in order to balance the weight of the droplet [9, 12]. Under stable levitation, the droplet center is shifted downwards from the pressure node by Z_{cg}. Consequently, the pressure distributions at the pole and equator are $P_{pole} = P_{\max}\sin\left(k_z(z_{cg} - b)\right)$ and $P_{eq} = P_{\max}\sin\left(k_z z_{cg}\right)J_0(k_r a)$ respectively. It can be shown that a change in aspect ratio by δc will induce changes in Bernoulli pressure at the pole and equator and are given by $\delta P_{pole} = \left[P_{\max}k_z\cos\left(k_z(z_{cg} - b)\right)\right]\frac{2b}{3c}.\delta c$ and $\delta P_{eq} = -\left[P_{\max}k_r\sin\left(k_z z_{cg}\right)J_1(k_r a)\right]\frac{a}{3c}\delta c$.

Thus, an increase in aspect ratio, i.e., δc,will reduce the radius of curvature at the equator, (negative δR_c) and increase the Bernoulli pressure at the pole. This, in turn, will create a fluid flow from the pole to the equator, increasing the liquid pressure near the equator. A positive δc will also decrease the Bernoulli pressure at the equator. Thus, a positive δc will result in an increase in Bernoulli pressure (P_{pole}-P_{eq}). In other words, change in aspect ratio shifts the droplet from equilibrium condition through changes in geometry and pressure distribution around the droplet. The relative changes of R_c and external pressure distribution (P_{pole}-P_{eq}) along the droplet surface dictate the stability of the droplet. For a small positive δc, the surface tension force increases and counteracts the increased Bernoulli pressure. Thus the droplet is normally restored to its original shape and exhibit some oscillation in aspect ratio about a mean value. In low surface tension fluids, higher deformation and oscillation of the droplet aspect ratio can be observed, although low surface tension does not always critically deform the droplet and lead it to catastrophic breakup. Normally, the shape oscillations are dissipated or damped quickly by viscosity. However, in cases where surface tension and viscosity are both low, the droplet can exhibit a propensity to approach the critical deformation limit due to high inhomogeneous Bernoulli pressure. It is important to note that the levitated droplet does not exhibit any shape oscillations in the unheated condition under the same acoustic loading. This implies when the droplet is heated, surface tension and viscosity decrease with temperature leading to potentially unstable situation. Figure 1 shows that the temperature continues to rise for ~0.2sec before it reaches a steady state value. Increase in temperature triggers a decrease in surface tension thereby, disturbing the equilibrium. In order to regain stability, the droplet tries to reshape itself with a lower radius of curvature (R_c) at the equator.

Stability parameter:

P_{pole} and P_{eq} are two extreme values of Bernoulli pressure acting on the levitated droplet. In a levitated droplet $\frac{\sigma}{R_c}$ represents the maximum surface tension pressure on the droplet- air interface as R_c represents the minimum radius of curvature on the droplet surface. So, we can define a parameter $\frac{(P_{pole}-P_{eq})R_c}{\sigma}$ as the ratio of the external acoustic pressure forces around the droplet and the maximum surface tension force on the droplet surface. This quantity represents an index for equilibrium between the external acoustic pressure field and surface tension forces at the droplet equator. Initially when the droplet is in equilibrium, we expect this parameter to be close to 1. With heating, surface tension decreases, resulting in an increase in aspect ratio, and also the force distribution. A small change in aspect ratio increases the (P_{pole}– P_{eq}) which in turn increases the aspect ratio and corresponding reduction R_c. If both of these changes are of the same order, the droplet retains its mean shape and does not undergo stretching or deformation. However, for kerosene droplet, the change in pressure force ($P_{pole} - P_{eq}$) is stronger compared to the increase in surface tension force (σ/R_c) due to the reduction in R_c. As explained in previous section, depending on the relative changes in these parameters and the damping coefficient, ζ, either the droplet remains near equilibrium or it stretches. If the droplet stretches it will imply $\frac{(P_{pole}-P_{eq})R_c}{\sigma}_{>1}$. If $\frac{(P_{pole}-P_{eq})R_c}{\sigma} \approx 1$ or initial, value (<1), then the droplet will retain its shape. However, $\frac{(P_{pole}-P_{eq})R_c}{\sigma} \gg 1$ implies monotonic increase in the aspect ratio, i.e., continuous stretching of the droplet.

By analogy of the aerodynamic break up, we can define a modified Weber number as $We_{TAB} = \frac{(P_{pole}-P_{eq})R}{\sigma}$. Thus the stability parameter defined in this section can be written as, $We_{TAB}R_c^*$ .It is important to mention here that the Weber number used here is based on the aerodynamic breakup modeled by using Taylor Analogy Breakup (TAB). This We_{TAB} is therefore different than Weber number (We_{eff}) used for KH instability analysis. The latter is used for characterizing global force balance for the successful levitation and it is based on the RMS value of the acoustic pressure (RMS of pressure distribution around the droplet) acting around the droplet and does not account for the increasing inhomogeneity of the pressure distribution due to shape change, which is important for analyzing localized instability such as oscillation in aspect ratio.

Our observation has been that among the liquid droplets, only kerosene undergoes significant distortion and eventual breakup. Therefore, we consider the viscous damping effect next.

Viscous Damping Effect:

In order to characterize the principal frequency modes of the change in aspect ratio observed for different liquids, Fast Fourier Transform (FFT) was performed for each droplet. FFT of the transient aspect ratio data for all droplets shows the presence of a few harmonic modes at some specific frequencies of 125 Hz, 250 Hz, 300 Hz etc. Although the higher frequencies are absent in some fuels, 125 Hz seems to be the omnipresent frequency for all fuels. This frequency was confirmed for water-based solutions as well. The large amplitude for kerosene also suggests that the oscillation is strongest for kerosene compared to other fuels.

The change in aspect ratio can be expressed as a series solution, $c(t) = \bar{c}(t) + \sum_i c_i'(t).\sin(2\pi f_i t)$, where $\bar{c}(t)$ denotes the bulk or mean (slow variation with time) variation in aspect ratio and $c_i'(t)$ denotes the change in aspect ratio due to different energy carrying capillary modes.

$\bar{c}(t)$ can be modeled by Taylor Analogy Breakup hypothesis [13], as this stretching and increase in aspect ratio is predominantly caused by the significant time varying inhomogeneity in the acoustic pressure distribution i.e. the pressure difference between the pole and equator, which tries to deform the droplet while surface tension acts as a spring with a certain stiffness and tries to retain the spherical shape. The viscosity acts as a damping mechanism to attenuate the stretching of the droplet.

Using simplified formulation of TAB model, we can write the damping ratio for $\bar{c}(t)$ is $\zeta = \frac{C_d}{2\sqrt{C_k}}\sqrt{\frac{\mu^2}{\sigma\rho R}} = \frac{C_d}{2\sqrt{C_k}}Oh$ where Oh is the Ohnesorge number. The damping time scale (for attenuation of the

droplet deformation), can be expressed as, $\tau_d = \frac{2}{C_d}\frac{\rho R^2}{\mu_l}$, where C_k and C_d are proportionality constants in the TAB model and considered to be constant for different fuel droplets. The transient variation of the damping ratio ($\frac{Oh}{2}$) as illustrated in Figure 5a, shows that it is weakest for kerosene. The damping timescale (Figure 5b) is also found to be highest for kerosene, indicating slow attenuation of the droplet deformation due to external acoustic pressure. FFT results and Figure 5, in summary, show that not only kerosene exhibits the highest amplitude in aspect ratio oscillation but also it has a low damping ratio leading to a large damping timescale.

The changes in $c_i'(t)$ is due to surface capillary waves on the droplets. Using theory of Capillary surface wave [14] it can be shown that the damping of the surface wave at all principal modes (fast varying energy containing capillary modes) is high during stage I of the droplet deformation process. The energy and the intensity of a damped capillary wave can be expressed as $\overline{I(t)} = \bar{I}_0.e^{-2C_{damp}t}$ where I is amplitude of the capillary waves [14]. The damping ratio coefficient $C_{damp} = 2\frac{\mu\omega^{4/3}}{\rho^{1/3}\sigma^{2/3}}$., where ω is the angular frequency of the oscillation of the droplet shape. The quantity, c' can be written as $c_i'(t) = c_0'.e^{-2C_{damp}t}$. From high speed images c'_i (t) can be expressed as $c_i'(t_{n+1}) = c_i'(t_n).e^{-2C_{damp}(t_{n+1}).(t_{n+1}-t_n)}$ where n is the frame number of high speed images. Using C_{damp} the instantaneous intensity (c' (t)) of oscillation for four fuels is calculated. It has been observed that the damping time scale for this capillary wave oscillation is in the order of 0.05 sec by which time the amplitude reduces by 90%. This oscillations (c') in aspect ratio in stage I is not very strong as the change takes place over 0.4 sec (Figure 4). On the other hand this oscillation (c') becomes important in Stage II and III when the pertinent timescale leading to breakup is of the order of 0.01 sec.

If ζ and C_{damp} for any fuel is very high, then the thermally induced oscillations in aspect ratio will dissipate faster even when $We_{TAB}R_c^* > 1.0$. In those cases, the droplet never approaches the critical deformation limit needed for bag type breakup. We may conclude the for the droplet to become critically unstable, two criteria must be satisfied together, 1) $We_{TAB}R_c^* > 1.0$ and 2) low ζ and C_{damp}. The first condition will initiate strong oscillation in aspect ratio and the latter will reduce the chances of damping that oscillation. Together these two conditions are necessary for droplet to oscillate beyond a critical limit and experience a catastrophic breakup.

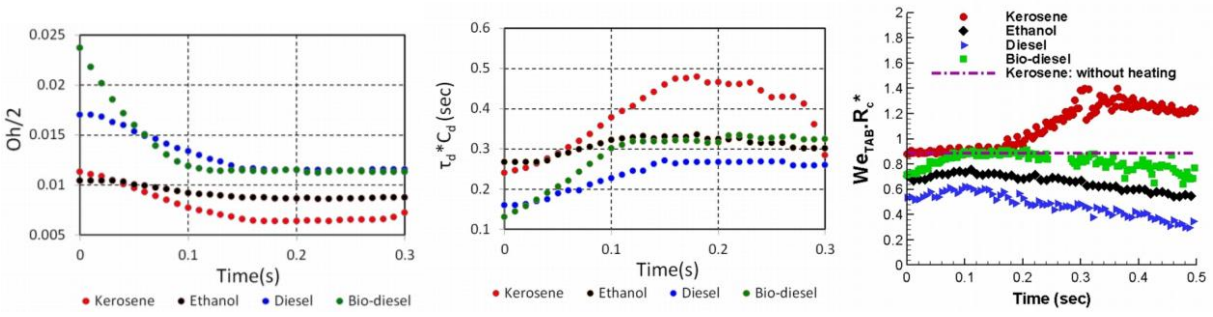

a) b) c)

Figure 5: a) Damping ratio (Oh/2) and b) damping timescale ($\tau_d C_d$) of aspect ratio ($\bar{c}$) oscillation as a function of time. C) Stability parameter ($We_{TAB}R_c^*$) as a function of time

The data in Figure 5c represents the true experimental conditions that include oscillations and viscous damping. It shows that for diesel, ethanol and bio-diesel, the parameter $We_{TAB}R_c^*$ initially increases only marginally with time and then decreases due to viscous damping. With increase in temperature, the droplet stretches and increases $We_{TAB}R_c^*$, but due to corresponding increase in surface tension force and due to viscous damping, the droplet shape returns to equilibrium. On the other hand for kerosene, the droplet stretches beyond a controllable limit with little resistance due to low viscous damping, hence, the parameter $We_{TAB}R_c^*$ increases monotonically and obtains a value of 1.4 which is much higher than 1.0.In a separate experiment we have observed that FC43 also displays uncontrollable stretching and bulk breakup like kerosene. Further calculation shows for FC43 the initial value of $We_{TAB}R_c^*$ is 0.92 while at the point of

catastrophic breakup the value is 1.33. In absence of heating the kerosene droplet maintains its equilibrium shape since the criteria $We_{TAB}R_c^* > 1.0$ is not satisfied.

Stage II and III:

After the droplet stretches beyond the critical value in the stage I, it morphs into a disk/membrane shaped structure. The Bernoulli pressure acting on this membrane tries to stretch it along the levitator axis or axis leading to the formation of a bag type structure. In stage III this sudden expansion in the perpendicular direction inflates the disk shaped liquid film and eventually disintegrates. One more important phenomenon we observe is that during the stretching and bag type break up process, the surface of the disk shaped liquid film shows small capillary waves. The tip of these small capillary waves which are moving around the droplet surface disintegrates to form small droplets.

Summary and Conclusions

This analysis shows that the observed secondary atomization in levitated fuel droplets is due to thermal effects. Since the density of fuels tested are close to each other, properties such as vapor pressure, latent heat and specific heat govern the vaporization rate and temperature history, which affect the surface tension gradient and gas phase density, ultimately dictating the onset of KH instability. High surface temperatures achieved in diesel, bio-diesel and kerosene favor small scale atomization through KH instability. High surface temperatures achieved in diesel, bio-diesel and kerosene favor small scale secondary atomization. The temperatures for fuels having high vapor pressure and high latent heat remain rather low and these droplets tend to be more stable like ethanol due to lower surface tension gradient.

In addition to the small scale atomization through KH instability, a second type of instability occurs in kerosene (also in FC 43) droplet due to a decrease in surface tension and viscosity with temperature. The change in surface tension causes the droplet to flatten due to increased Bernoulli pressure at the poles resulting in an increase in aspect ratio. The imbalance in pressure force and surface tension force near the equator creates shape oscillation. If the viscous damping of this oscillation is not strong enough, the droplet goes through unbounded stretching morphing into a disk-like object, followed by a bag type catastrophic breakup. Analysis shows there are two important parameters which dictates inception of this instability. A parameter $We_{TAB}R_c^*$ represents relative strength of Bernoulli pressure to surface tension, where the former is responsible for stretching the droplet and the latter acts as stiffness of the droplet. Other important parameter is viscous damping or damping ratio, which is a function Ohnesorge number, Oh. A criterion for catastrophic breakup of droplet is obtained as $We_{TAB}R_c^* > 1$ and a low damping ratio as represented by Ohnesorge number. In a containerless levitated droplet, KH instability always precedes this second type of instability. These instabilities arise due to external heating and temperature dependent properties of the liquid fuels, and cannot occur due to natural drying alone.

References

[1] Lieuwen T. (2001) Theoretical investigation of unsteady flow interactions with a premixed planar flame J. Fluid Mech., 435, 289-303

[2] Qi A., Yeo L. Y. & Friends J. R., (2008) Interfacial destabilization and atomization driven by surface acoustic waves, Phys. Fluids, 20, 074103

[3] Yarin A. L., Pfaffenlehner M. & Tropea C. (1998) On the acoustic levitation of droplets, J. Fluid Mech., 356 65-91

[4] Saha A., Basu S., Suryanarayana C. & Kumar R (2010) Experimental analysis of thermo-physical processes in acoustically levitated heated droplets, Int. J. Heat and Mass Transfer, 53, 5663-5674

[5] Saha A., Basu S. & Kumar R. (2012) Particle image velocimetry and infrared thermography in a levitated droplet with nanosilica suspensions Exp. in Fluids, Exp. Fluids 52, 795-807

[6] Kumar R., Tijerino E., Saha A. & Basu S. (2010) Structural morphology of acoustically levitated and heated nanosilica droplet App. Phys. Lett., 97, 123106-1-3

[7] Lobdell, D.D. (1968) Particle size-amplitude reactions for the ultrasonic atomizer, J. Acoust. Soc. Am., 43, 229-231

[8] Anilkumar A. V., Lee C. P. & Wang T. G. (1993) Stability of an acoustically levitated and flattened drop: An experimental study, Phy. Fluids., 5, 2763

[9] Lierke E. G. (2002) Deformation and displacement of liquid drops in an optimized acoustic standing wave levitator, Acta Acoustica United with Acoustica., 88, 206-217

[10] Chandrashekhar S., Hydrodynamic and Hydromagnetic Stability, (Dover Publications, New York, 1981)

[11] W. A. Sirignano, Fluid Dynamics and Transport of Droplets and Sprays (Cambridge University press, New York, 2010), 2nd ed

[12] Saha A., Basu S. & Kumar R. (2012) Effect of acoustic-streaming-induced flow on vaporizing nanofluid droplet J. Fluid Mech., 692, 207-219

[13] O'Rourke P. J. & Amsden A. A. (1987) The TAB Method for Numerical Calculation of Spray Droplet Breakup, SAE Technical Paper, paper no. 872089

[14] Landau L. D. & Lifshitz E. M. (1987) Fluid Mechanics Butterworth-Heinemann,